
Article:
Jones, N.G., Izzo, R., Mignanelli, P.M. et al. (2016) Phase evolution in an Al0.5CrFeCoNiCu High Entropy Alloy. Intermetallics, 71. pp. 43-50. ISSN: 0966-9795

https://doi.org/10.1016/j.intermet.2015.12.001

Intermetallics 71 (2016) 43–50

Contents lists available at ScienceDirect

Intermetallics

journal homepage: www.elsevier.com/locate/intermet

Phase evolution in an $Al_{0.5}CrFeCoNiCu$ High Entropy Alloy

N.G. Jones*, R. Izzo, P.M. Mignanelli, K.A. Christofidou, H.J. Stone

Department of Materials Science and Metallurgy, University of Cambridge, 27 Charles Babbage Road, Cambridge, CB3 0FS, UK

ARTICLE INFO

Article history:
Received 25 September 2015
Received in revised form
17 November 2015
Accepted 9 December 2015
Available online 8 January 2016

Keywords:
High-Entropy Alloys
Phase transformation
Heat treatment
Electron microscopy
Scanning

ABSTRACT

The phase evolution of an $Al_{0.5}CrFeCoNiCu$ High Entropy Alloy has been characterised following isothermal exposures between 0.1 and 1000 h at temperatures of 700, 800 and 900 °C. The NiAl based B2 phase formed extremely quickly, within 0.1 h at the higher exposure temperatures, whilst the Cr-rich σ phase formed more slowly. The solvus temperatures of these two phases were found to be ~975 and ~875 °C respectively. Compilation of the data presented here with results previously reported in the literature enabled the production of a time-temperature-transformation diagram, which clearly indicates that the diffusion kinetics of this material cannot be considered sluggish.

1. Introduction

High Entropy Alloy (HEA) systems have been the subject of extensive research since their inception just over a decade ago. A huge number of different alloys have already been studied and several beneficial properties identified, including good mechanical, wear and corrosion characteristics [1–6]. However, due to the compositionally complex nature of these materials, the development of optimal alloy chemistries will only be realistically possible via high-throughput computational and experimental techniques [7–10]. Efficient use of such techniques requires an improved understanding of the fundamental mechanisms behind the behaviour of these materials, which can only be achieved through systematic studies of the compositional and processing dependence of key material properties.

The multi-element basis of HEAs has been reported to give rise to a number of key benefits over their conventional, single element based counterparts [11–14]. These effects include; increased entropies of mixing, which improve the structural stability, particularly at elevated temperatures, suppressing the formation of undesirable embrittling intermetallic phases [11,12]; severely distorted crystal lattices, which are thought to be responsible for the low thermal and electrical conductivity of these materials, as well as providing strengthening by impeding dislocation movement, and; sluggish diffusion kinetics, which gives rise to low grain growth rates and enhanced creep resistance. However, despite the considerable number of research studies published to date, the validity of these underlying principles has not yet been conclusively established.

Slow diffusion in HEAs is thought to be a direct consequence of the complex arrangement of atoms of different elemental species. In a conventional, single element dominated solid solution, the bonding conditions of the local neighbourhood prior to, and following a solute atom jump are essentially equivalent. The same is not true in an HEA, where the local atomic configuration is expected to vary considerably from site to site. As a result, it has been suggested that a diffusing species may become trapped at lower energy sites or rejected by higher energy sites, both of which would retard atomic motion [14]. Calculations have shown that for a migrating Ni atom the difference in lattice potential energy between sites is greater in an CrMnFeCoNi HEA than it is in Fe–Ni–Cr austenitic steels, which implies slower rates of diffusion in the HEA [15]. A series of quasi-binary diffusion couples were used to determine the activation energies of diffusion for each elemental species in CrMnFeCoNi [15]. Whilst the activation energies of some species were slightly higher in the HEA than those previously reported in Fe, Ni, Co or austenitic Fe–Ni–Cr alloys, the activation energies of other species were lower. Normalisation of these data with the alloy's melting temperature, and extrapolation to obtain the diffusion coefficients near melting, did indicate that diffusion was slowest in the HEA, although none of these values can be considered anomalously low.

* Corresponding author.
E-mail address: ngj22@cam.ac.uk (N.G. Jones).

http://dx.doi.org/10.1016/j.intermet.2015.12.001

The nucleation and growth of a new phase requires long range coordinated inter-diffusion of the different elemental species and, therefore, would not be expected to occur quickly in materials with low diffusion coefficients. However, rapid precipitation has been reported in some HEAs, including the observation of a fine scale spinodal microstructure in $Al_{0.5}CrFeCoNiCu$ following rapid cooling [16,17] and evidence has been obtained that this phase separation occurs even when cooling at rates that approach 1 °C s^{-1} [18]. Thus, it would appear that diffusion is not universally slow in all HEAs.

Previous work has established the presence of multiple phases within the microstructure of $Al_{0.5}CrFeCoNiCu$ following long-term heat treatments at temperatures between 700 and 1000 °C. These include a NiAl based B2 phase, the topologically close packed σ phase and an Ni_3Al based $L1_2$ phase, in addition to two *fcc* solid solutions [19–21]. However, little is known about the speed at which these phases form, information that is intrinsically linked to the diffusion kinetics of the alloy. Therefore, to address this issue, the phase evolution in $Al_{0.5}CrFeCoNiCu$ has been studied following a series of different exposure times at temperatures of 700, 800 and 900 °C, and the data used to construct a time-temperature-transformation diagram.

2. Experimental methods

A 500 g charge of $Al_{0.5}CrFeCoNiCu$ was melted in a vacuum induction furnace from elemental metals with purity ≥99.9%. The material was held in the molten state for ~30 min before being cast into six 10 mm diameter bars, which were ~100 mm in length. The as-cast bars were encapsulated in evacuated, Ar-backfilled glass ampoules and homogenised at 1100 °C for 96 h. This temperature was selected based upon previous reports, which indicated that the first melting event observed in this alloy occurred at ~1150 °C [20,21]. At the end of the homogenisation treatment, five of the bars were water quenched, whilst the remaining bar was air-cooled. The water quenched bars were sectioned into ~10 mm lengths, which were individually encapsulated as described above and exposed for periods between 0.1 and 1000 h at temperatures of 700, 800 and 900 °C. All samples were water quenched following thermal exposure.

The microstructures of the homogenised and heat-treated samples were characterised using back-scattered electron (BSE) imaging in an FEI Nova NanoSEM 450. Bulk and phase compositions, as well as elemental distribution maps, were obtained in the same instrument with a Bruker XFlash 6 solid-state energy dispersive X-ray (EDX) detector. Bulk compositions were obtained by averaging the data from several large area measurements, while phase chemistry was determined from several point analyses. Selected local crystallographic characterisation was performed using electron backscatter diffraction (EBSD) in the NanoSEM 450, whilst bulk information from all samples was collected using a Bruker D8 diffractometer with Ni-filtered Cu Kα radiation. Diffraction spectra were collected within the range 5–135° 2θ in 0.03° 2θ steps counting for 2 s per step and between 42 and 52° 2θ in 0.03° 2θ steps counting for 8 s per step. Differential Scanning Calorimetery (DSC) was used to obtain the solvus temperatures of the solid-state phase transformations that occurred during continuous heating from room temperature to 1400 °C. Measurements were performed in a Netzsch 404 calorimeter under flowing argon at a heating rate of 10 °C min^{-1}.

3. Results

The bulk composition of the cast material, determined by averaging large area EDX analyses at the top and bottom of each bar, is provided in Table 1. The measured composition of each element was within 1 at% of the target value in all cases except Al, which was found to be 1.8 at% below the nominal concentration. Al has a low vapour pressure and losses are expected during the melting process. In the current study, these losses were greater than expected, resulting in a slightly depleted concentration of Al in the final alloy. The bulk homogeneity of the material was very good, as can be seen by the low error values in Table 1, which correspond to the standard deviation between all of the different measurements.

Table 1
Target and measured composition of the material studied, with the standard deviation in measurements given as the error.

At.%	Cr	Fe	Co	Ni	Cu	Al
Target	18.2	18.2	18.2	18.2	18.2	9.0
Measured	19.1	18.7	18.6	18.2	18.2	7.2
Error	*±0.3*	*±0.1*	*±0.1*	*±0.1*	*±0.5*	*±0.2*

BSE micrographs of the material following the 96 h homogenisation treatment at 1100 °C in both the air cooled and water quenched states are shown in Fig. 1. In both conditions, the material had a dendritic microstructure, which is consistent with many previous studies [1,19–21]. In line with this previous work, EDX analysis showed that the dendrites were multi-component solid solutions, whilst the interdendritic constituent was Cu-rich. However, in the air cooled material, acicular precipitates could be seen within the interdendritic regions. Elemental mapping indicated that these phases were rich in Ni and Al, and, therefore, were likely to be the B2 NiAl phase [19–21]. Similar features were not observed in the water quenched material, suggesting that diffusion in the interdendritic phase was sufficiently fast to allow elemental redistribution, leading to precipitation of the B2 phase during air cooling. As a result, only material that had been water quenched from the homogenisation treatment was used in the remaining part of this study.

Images showing the microstructural evolution of $Al_{0.5}CrFeCoNiCu$ as a function of exposure time at 700, 800 and 900 °C are given in Fig. 2[1]. After exposure for 1 h at 700 °C, fine globular precipitates were observed in the microstructure that were not present in either the as-quenched material or following 0.1 h at 700 °C. These precipitates, labelled as *a* in Fig. 2, were observed to preferentially form on the grain boundaries within the dendritic microstructure. EDX analysis showed that the precipitates were rich in Ni and Al, consistent with the B2 phase previously reported [19,21]. In addition to the globular phase, small acicular precipitates, labelled as *b* in Fig. 2, with similar backscattered electron contrast were also observed within the interdendritic material. The fine scale of these precipitates meant that accurate compositional analysis was challenging but elevated levels of Ni & Al were measured, which, in keeping with previous work [19,21], suggested that these precipitates were also the B2 phase. Following 10 h at 700 °C, the occurrence of acicular B2 precipitates within the interdendritic regions had become extensive, with individual precipitates extending across the entire width of the interdendritic regions. Additional fine precipitates, with similar morphology and backscattered contrast to those in the interdendritic regions, were observed within the dendritic phase after exposure for 50 h, labelled as *c* in Fig. 2. Thus, within 50 h exposure to 700 °C, three different populations of the B2 phase were observed to have formed in $Al_{0.5}CrFeCoNiCu$; globular precipitates on the grain boundaries, acicular precipitates within the interdendritic phase and acicular precipitates within the dendrites. With longer

[1] Larger versions of each individual image within Fig. 2 are provided as online supplementary information.

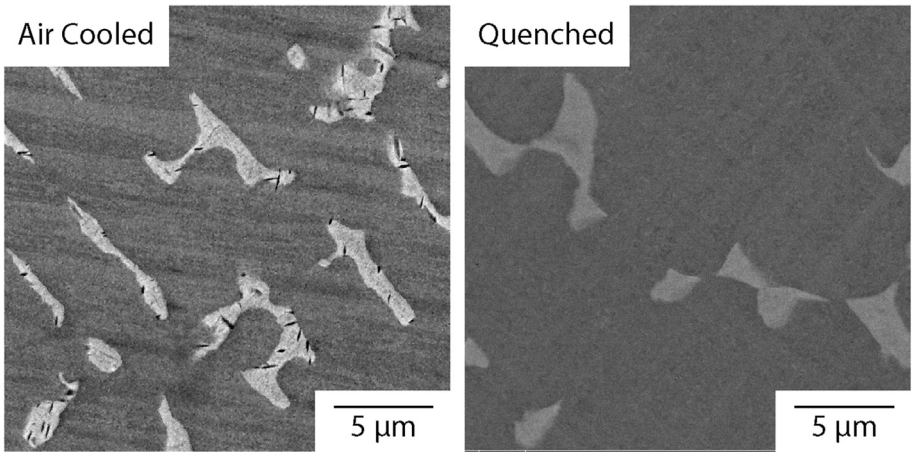

Fig. 1. BSE micrographs of $Al_{0.5}CrFeCoNiCu$ after heat treatment at 1100 °C for 96 h followed by air cooling and water quenching.

exposure times, all three populations of the B2 phase coarsened and an increase in volume fraction was observed. This was particularly true of the acicular precipitates within the dendritic regions, which dominated the microstructure after 1000 h. During this time, another intermetallic precipitate was also observed to have formed. Following a 100 h exposure, regions of material that had similar backscattered electron contrast to the original dendrites were observed, labelled as *d* in Fig. 2, but, critically, unlike the dendritic material, these regions were free from any internal precipitation. EDX analysis of these areas showed significantly elevated Cr concentration, consistent with previous reports of the σ phase at this temperature [19,21]. Phase mapping, using concurrent EDX and EBSD, was performed on material exposed for 1000 h at 700 °C and confirmed that all of the Ni and Al rich regions had a B2 crystal structure and that the Cr rich areas were tetragonal, consistent with the σ phase.

At 800 °C the phase evolution of $Al_{0.5}CrFeCoNiCu$ with exposure time followed the same general trend as that at 700 °C, although there were some key differences. The formation of globular B2 on the grain boundaries and the precipitation of acicular B2 within the interdendritic material occurred more rapidly, within the first few minutes of exposure, with both of these features evident in the micrograph following a 0.1 h exposure. Similarly, acicular B2 precipitates were observed within the multi-component dendrites following 1 h at 800 °C. This was considerably faster than at 700 °C, where the acicular intradendritic precipitates were observed to form between 10 and 50 h. In addition, the acicular B2 precipitates formed within the dendrites at 800 °C appeared to be fully developed following a 10 h exposure and coarsened with longer exposure times. The Cr-rich σ phase was also found to form at shorter exposure times at 800 °C than was observed at 700 °C. Evidence of its presence was found in the microstructure following a 10 h exposure at 800 °C, as can be seen in the EDX maps shown in Fig. 3. Despite a lack of backscattered contrast, the elemental partitioning maps clearly show regions with an elevated concentration of Cr, which also contain Fe and Co, next to the globular B2 precipitates. Regular arrays of fine scale bright precipitates were also seen within the dendrites following exposure for 10 h at 800 °C, Fig. 4. These features became more apparent as the exposure time increased and they coarsened. It is believed that these precipitates are Cu rich and form as a result of the miscibility gap in this system [20] and their formation is consistent with the nano-scale spinodal decomposition of the multi-component dendrites previously observed in this alloy [16,18].

At short exposure times, up to an hour, the phase evolution at 900 °C was similar to that observed at 800 °C. However, in contrast to the material exposed at 800 °C, all three populations of the B2 phase, globular grain boundary, acicular in the interdendritic constituent and acicular in the dendritic regions, were observed following 0.1 h at 900 °C. In addition, an extremely fine scale regular array of bright contrast precipitates could be seen within the dendrites after a 1 h exposure, Fig. 5. As can be seen in Fig. 2, this three-phase microstructure coarsened with increasing exposure time, but at no stage was any evidence of the σ phase observed. This finding is consistent with previous reports that have indicated that the σ solvus temperature must lie between 850 °C, where σ has been reported following a 1000 h exposure [21], and 900 °C [19].

Full X-ray diffraction spectra, between 5 and 135° 2θ, were acquired from material in all heat treatment conditions. However, it was found that the reflections within the range 42 and 52° 2θ provided the most concise evidence of phase evolution. The spectra for the different times at each exposure temperature are shown in Fig. 6, along with the spectrum from the homogenised and water quenched starting material, identified as an exposure time of 0 h. In the spectrum obtained from the homogenised material, only peaks corresponding to an *fcc* structure were observed, but, in keeping with previous work [1,19–21], the shape of line profile of these reflections indicated that they resulted from multiple *fcc* based structures, all with similar lattice parameters. B2 reflections were observed in the XRD spectra following a 1 h exposure at 700 °C and 0.1 h exposures at 800 and 900 °C, consistent with the electron microscopy results presented in Fig. 2. The separation of the two main *fcc* reflections, the multi-component solid solution and the Cu-rich phase, is well captured in the XRD spectra and provides some qualitative information about the effect of temperature on the diffusion rates in $Al_{0.5}CrFeCoNiCu$. Reflections corresponding to the σ phase were also present in the XRD spectra following exposure at 700 and 800 °C but not at 900 °C. Their occurrence is in keeping with the electron microscopy results but the exposure time after which they can be discerned does not correlate so well. From the XRD spectra, reflections corresponding to the σ phase were present following a 1000 h exposure at 700 °C and after 50 h at 800 °C. In contrast, microstructural evidence of this phase was detected in the elemental partitioning maps obtained from material following shorter exposure times, 100 h at 700 °C and 10 h at 800 °C. It is believed that the localised probing possible with electron microscopy enabled identification of the σ phase at an earlier stage of its formation, corresponding to a volume fraction below the detection limit of the XRD equipment used.

A DSC thermogram obtained from $Al_{0.5}CrFeCoNiCu$ following

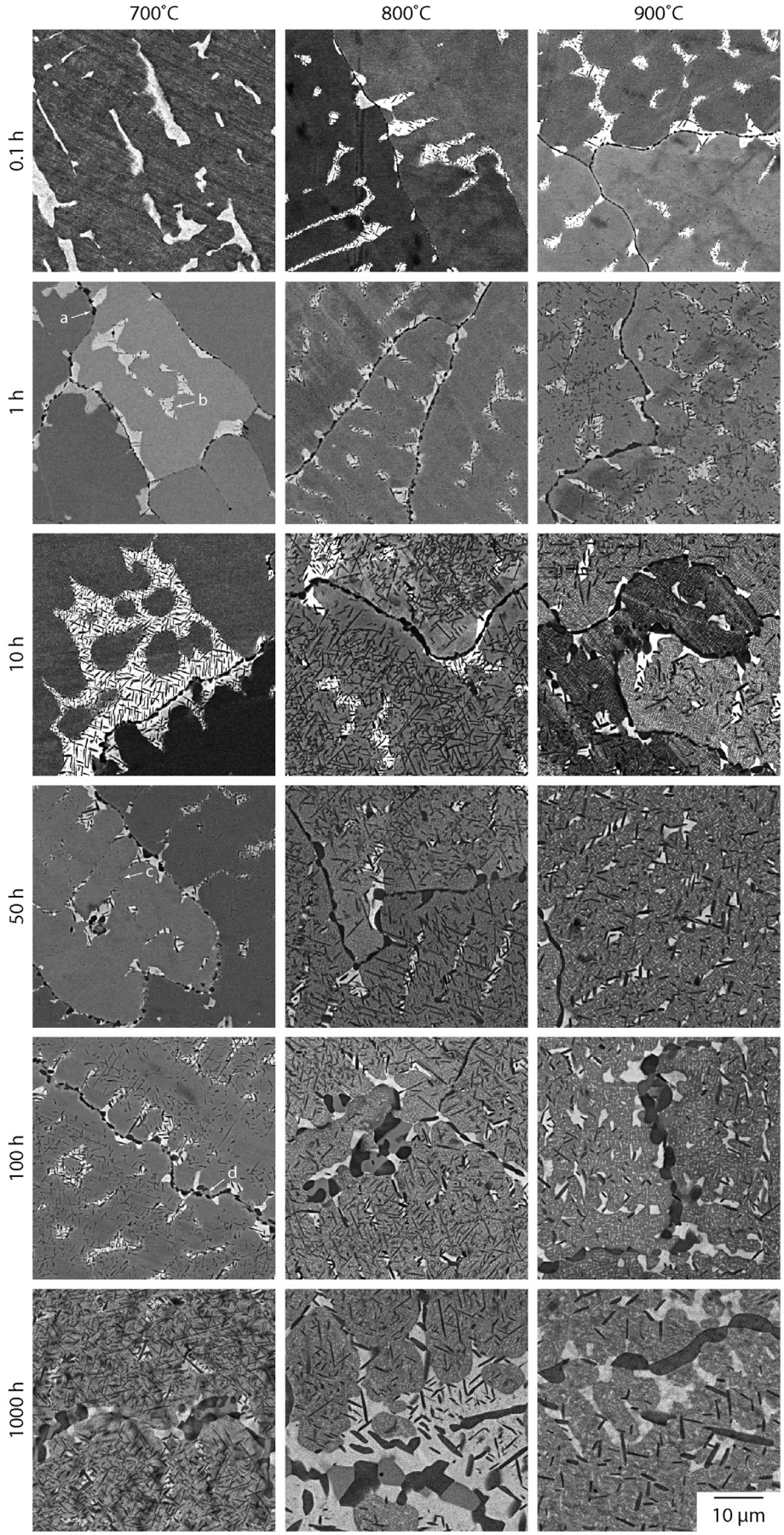

Fig. 2. BSE micrographs of $Al_{0.5}CrFeCoNiCu$ following thermal exposure at 700, 800 and 900 °C for times between 0.1 and 1000 h.

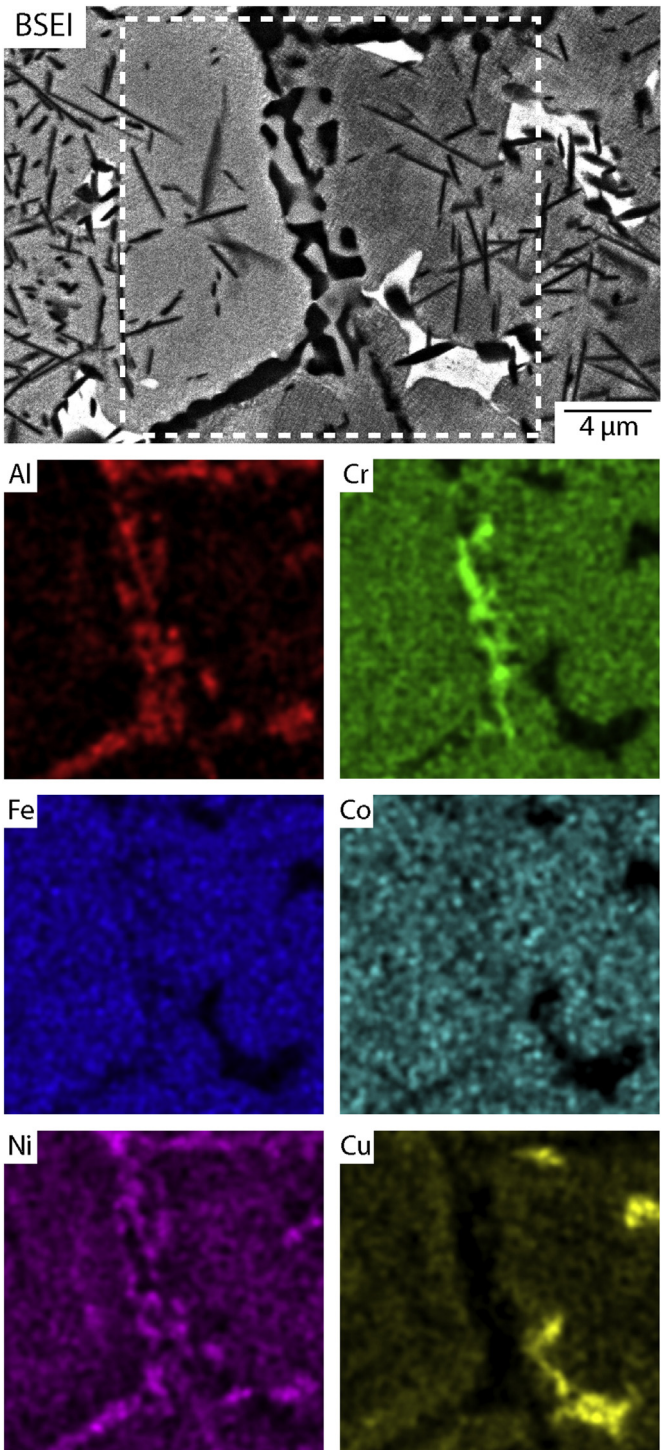

Fig. 3. BSE micrograph and corresponding EDX elemental partitioning maps showing the detection of the σ phase in $Al_{0.5}CrFeCoNiCu$ following heat treatment for 10 h at 800 °C.

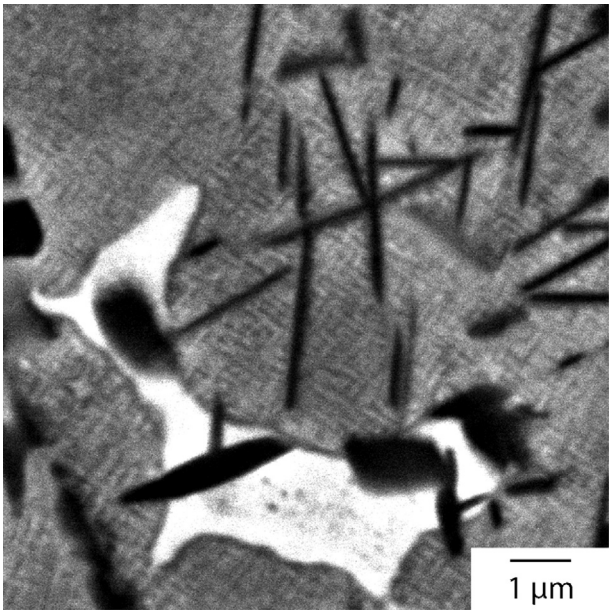

Fig. 4. High magnification BSE micrograph of $Al_{0.5}CrFeCoNiCu$ following 10 h at 800 °C showing the regular arrays of bright precipitates within the dendrites.

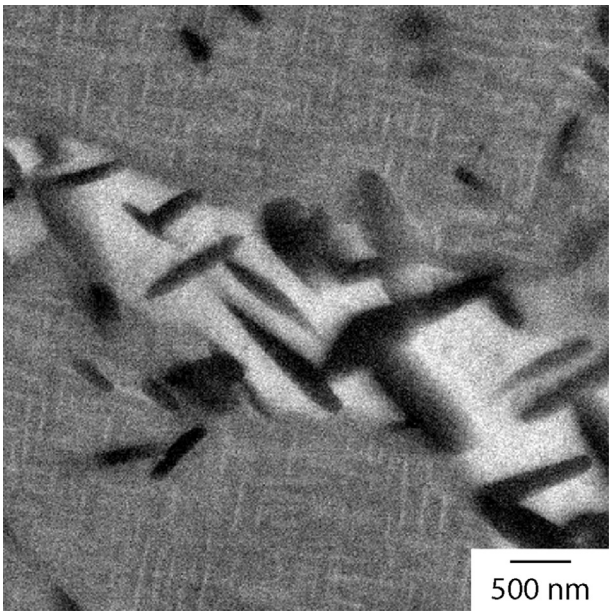

Fig. 5. High magnification BSE micrograph of $Al_{0.5}CrFeCoNiCu$ following 1 h at 900 °C showing the bright fine scale decomposition product within the grey multi-component dendrites.

exposure for 1000 h at 900 °C is shown in Fig. 7. Microstructural characterisation and XRD analysis of this material indicated that only the two *fcc* parent phases and the B2 precipitates were present. The thermogram shows four distinct events that occur between 600 and 1400 °C; two large endothermic peaks at ~1350 and ~1150 °C and two sigmoidal like deviations which finish at ~975 and ~800 °C respectively. Previous studies have shown that the two highest temperature events correspond to the melting of the dendritic and interdendritic constituent, whilst the lowest temperature event is related to a non-equilibrium $L1_2$ phase that forms during cooling [18,20,21]. These studies also established that only the two *fcc* phases are present following 1000 h at 1000 °C and thus it is believed that the sigmoidal deviation finishing at ~975 °C corresponds to the B2 solvus temperature. This is in good agreement with previous unpublished work, where the microstructure of arc melted $Al_{0.5}CrFeCoNiCu$, which comprised of two *fcc* phases and $L1_2$ precipitates [16,20] in the as cast state, contained B2 precipitates following a 0.25 h exposure at 950 °C, Fig. 8.

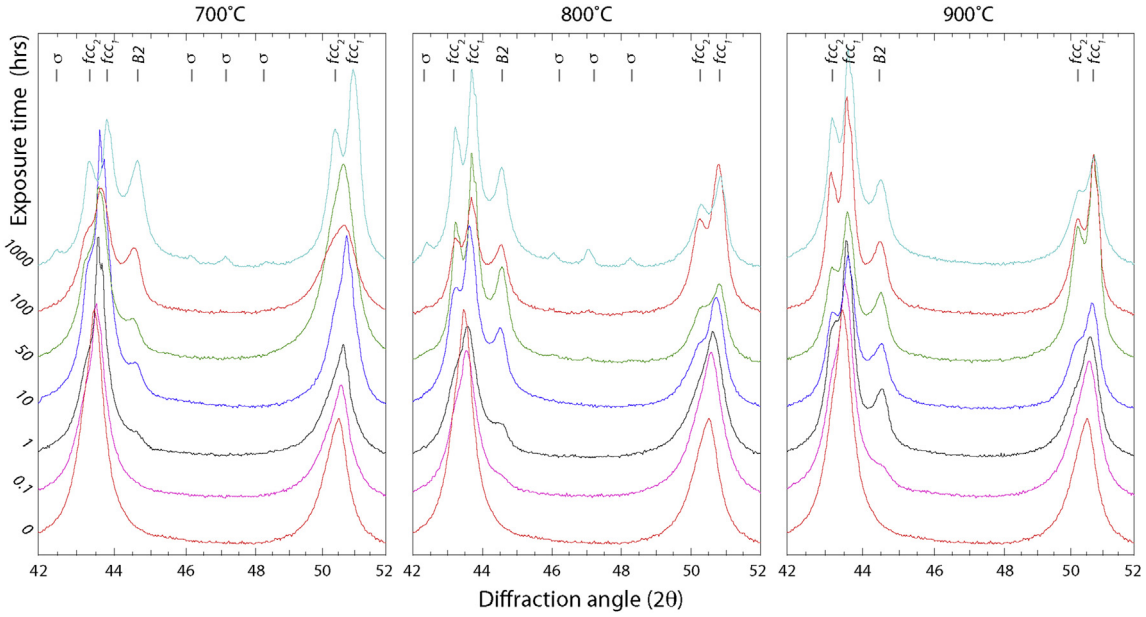

Fig. 6. X-ray diffraction spectra from $Al_{0.5}CrFeCoNiCu$ in the homogenised state and following thermal exposure at 700, 800 and 900 °C for times between 0.1 and 1000 h.

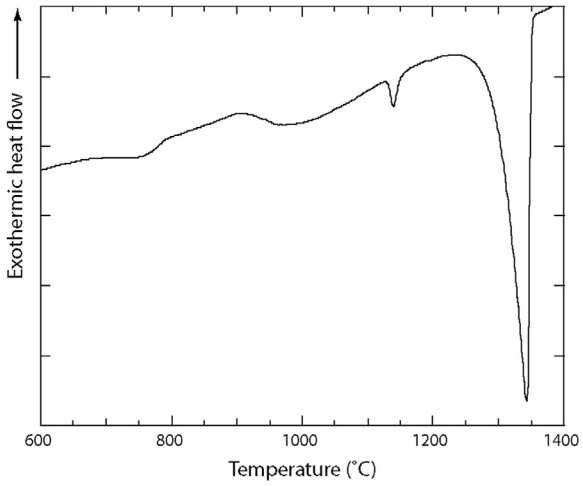

Fig. 7. DSC thermogram during heating of $Al_{0.5}CrFeCoNiCu$ following 1000 h at 900 °C.

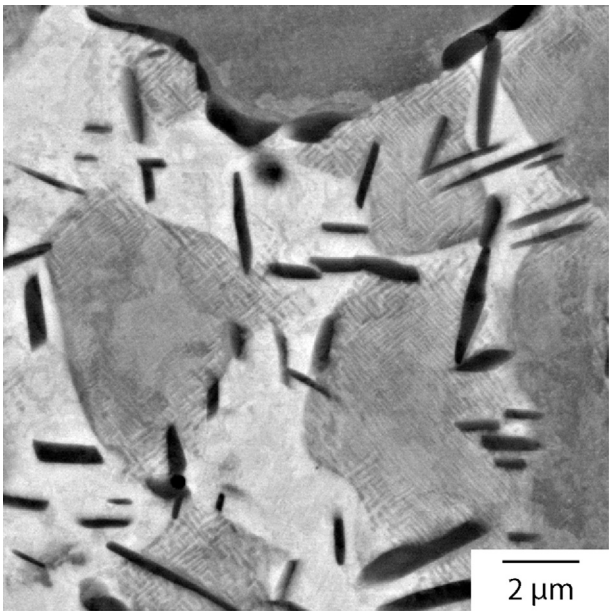

Fig. 8. BSE micrograph of as arc melted $Al_{0.5}CrFeCoNiCu$ following exposure at 950 °C for 0.25 h showing the presence of the B2 phase.

4. Discussion

Compilation of the current experimental results with those already published in the literature allowed the construction of a time-temperature-transformation diagram for $Al_{0.5}CrFeCoNiCu$, Fig. 9. In this diagram, the filled symbols correspond to data collected during the present work, whilst the open symbols show data from previous studies. It should be noted that the $L1_2$, *fcc* superlattice phase, which is known to form in this alloy [1,16,17,19–21], has been omitted from this figure as no evidence has been obtained to indicate that its formation can be suppressed by rapid cooling. As such, post mortem examination of samples recovered from elevated temperature heat treatments cannot be used to unambiguously identify whether this phase was present at the exposure temperature or whether elemental partitioning between different phases in the evolving microstructure influences its occurrence.

It is clear that the B2 phase can form extremely quickly in this material, having been observed on prior grain boundaries and in the interdendritic constituent following 0.1 h exposures at 900 and 800 °C and after 1 h at 700 °C. However, its formation within the multi-component dendrites was slower and showed a significant dependence on the exposure temperature. Intradendritic B2 precipitates were observed following 0.1 h at 900 °C, 1 h at 800 °C and 50 h at 700 °C. Previously, micrographs have been published that show similar acicular precipitates within the dendrites following a 24 h exposure at 700 °C [19]. This observation is consistent with the current work, however, the result cannot be directly incorporated into Fig. 9 as, prior to exposure, the material had been cold rolled and annealed at 900 °C, during which time the B2 phase formed.

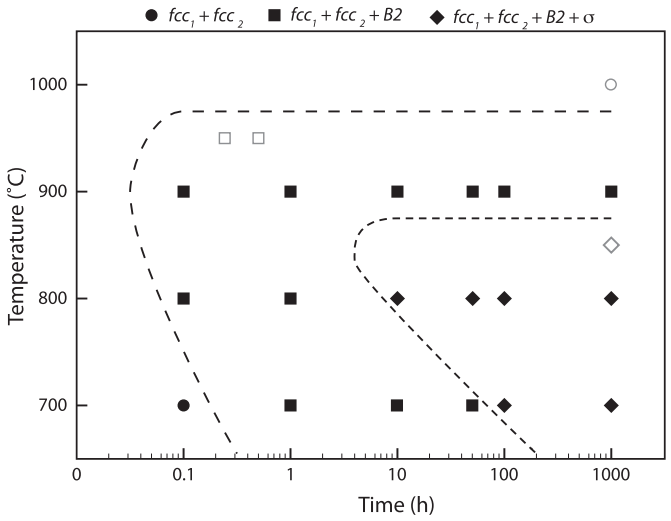

Fig. 9. Time-temperature-transformation diagram for $Al_{0.5}$CrFeCoNiCu. The filled points correspond to experimental results of the present work, open symbols represent data taken from Ref. [21] or previous unpublished data.

The structurally complex σ phase formed more slowly than the B2 phase in $Al_{0.5}$CrFeCoNiCu and had a lower solvus temperature, between 850 and 900 °C. In the present work, evidence of this phase was found after 10 h at 800 °C and following 100 h at 700 °C. Again, this observation is in slight disagreement with Ng et al. [19] who presented XRD spectra clearly containing characteristic σ reflections after only 24 h at 700 °C. As stated previously, this inconsistency is believed to be related to the fact that the material in Ref. [19] had been cold worked and annealed at 900 °C prior to exposure at 700 °C. The results of the present work have clearly demonstrated that the B2 phase forms at shorter exposure times than the σ phase. In addition, previous work [21], has shown that the B2 phase accommodates reasonable concentrations of Fe, Co & Cu, ~8, ~10 and ~10 at% respectively, at temperatures between 700 and 850 °C, but far less Cr, ~3 at%. Thus, the formation of the B2 phase would significantly enrich the surrounding material in Cr and this appears to destabilise the *fcc* phase with respect to intermetallic phase formation. This situation is exacerbated in the Cu-rich interdendritic material as Cr, Co and Fe are rejected as the phase moves towards its equilibrium composition from its metastable starting point, where only Ni and Al retain appreciable concentrations in solid solution [21]. Therefore, it is unsurprising that the σ phase is commonly observed adjacent to B2 precipitates, near or within the inderdendritic constituent. As a result, the formation of the B2 phase during interpass annealing at 900 °C in the material studied in Ref. [19] would have created areas within the material with elevated Cr concentrations, prior to exposure at 700 °C. The presence of such regions within the material whilst it is exposed at temperatures where the σ phase is stable, in addition to any remnant dislocations, would no doubt accelerate its formation, thereby accounting for the discrepancy between reference [19] and the present study.

As stated in the introduction, reconstructive phase transformations require cooperative movement of different atomic species over relatively large distances. The rapid formation of the B2 phase during both isothermal heat treatments, and air cooling from 1100 °C indicates that neither the nucleation kinetics nor the diffusional growth of this phase are sluggish in $Al_{0.5}$CrFeCoNiCu. The formation of the σ phase did require longer exposure times, particularly at 700 °C, but even then, these times are not disproportionally long when compared to other materials. For example, in relatively compositionally simple duplex stainless steels with similar Cr concentrations to $Al_{0.5}$CrFeCoNiCu, the σ phase has been reported to form very quickly at temperatures between 700 and 850 °C [22,23]. In contrast, within more compositionally complex materials, such as Ni-base superalloys, which again have comparable Cr contents, the σ phase requires several hundred hours to form at these temperatures [24,25]. Thus, whilst diffusion in HEAs is widely reported to be sluggish, the data presented here clearly shows that it is not anomalously slow in $Al_{0.5}$CrFeCoNiCu.

5. Conclusions

The phase evolution of an $Al_{0.5}$CrFeCoNiCu High Entropy Alloy has been characterised following isothermal exposures between 0.1 and 1000 h at temperatures of 700, 800 and 900 °C. In line with previous reports, the starting material contained two *fcc* phases and two additional intermetallic phases were observed to form during the thermal exposures, a NiAl based B2 phase and the more complex Cr-rich σ phase. The B2 phase, which had a solvus temperature of ~975 °C, formed extremely quickly in this material, within 1 h at 700 °C and in less than 0.1 h at 800 & 900 °C, as well as during air cooling from 1100 °C. The σ phase, which has a solvus of ~875 °C, formed more slowly than the B2, requiring between 1 & 10 h at 800 °C and 50 & 100 h at 700 °C. The formation of the σ phase is thought to be directly related to the destabilisation of the parent material around a B2 precipitate, as this phase has little solubility for Cr and so enriches the surrounding area. Combination of these data with existing results from the literature enabled a time-temperature-transformation diagram to be proposed for the first time. Since the formation of a new phase requires long range coordinated diffusion, the experimental observation of intermetallic phase formation within 0.1 h indicates that the diffusion kinetics within this High Entropy Alloy are not anomalously slow.

Acknowledgements

The authors would like to thank K. Roberts and S. Rhodes for their assistance, and the EPSRC/Rolls-Royce Strategic Partnership (EP/M005607/1 and EP/H022309/1) for funding. The original research data for this study can be found at https://www.repository.cam.ac.uk/handle/1810/252934.

Appendix A. Supplementary data

Supplementary data related to this article can be found at http://dx.doi.org/10.1016/j.intermet.2015.12.001.

References

[1] C. Tong, Y. Chen, S. Chen, J. Yeh, T. Shun, C. Tsau, S. Lin, S. Chang, Metall. And Mater. Trans. A 36A (2005) 881–893.
[2] Y.J. Zhou, Y. Zhang, Y.L. Wang, G.L. Chen, Appl. Phys. Lett. 90 (2007) 181904.
[3] O.N. Senkov, C. Woodward, D.B. Miracle, JOM 66 (2014) 2030–2042.
[4] C.Y. Hsu, J.W. Yeh, S.K. Chen, T.T. Shun, Metall. Mater. Trans. A 35 (2004) 1465–1469.
[5] P.K. Huang, J.W. Yeh, T.T. Shun, S.K. Chen, Adv. Eng. Mater. 6 (2004) 74–78.
[6] Y. Hsu, W. Chiang, J. Wu, Mater. Chem. Phys. 92 (2005) 112–117.
[7] D.B. Miracle, Mater. Sci. Technol. 31 (2015) 1142–1147.
[8] D. Miracle, J. Miller, O. Senkov, C. Woodward, M. Uchic, J. Tiley, Entropy 16 (2014) 494–525.
[9] O.N. Senkov, J.D. Miller, D.B. Miracle, C. Woodward, Nature Communications, 6(1) 1–10.
[10] F. Zhang, C. Zhang, S.L. Chen, J. Zhu, W.S. Cao, U.R. Kattner, Calphad 45 (2013) 1–10.
[11] J. Yeh, S. Chen, S. Lin, J. Gan, T. Chin, T. Shun, C. Tsau, S. Chang, Adv. Eng. Mater. 6 (2004) 299–303.
[12] J.-W. Yeh, Ann. de chimie Sci. des Materiaux 31 (2006) 633–648.
[13] J.-W. Yeh, JOM 65 (2013) 1759–1771.

[14] M.-H. Tsai, J.-W. Yeh, Mater. Res. Lett. 2 (2014) 107–123.
[15] K.Y. Tsai, M.H. Tsai, J.W. Yeh, Acta Mater. 61 (2013) 4887–4897.
[16] E.J. Pickering, H.J. Stone, N.G. Jones, Mater. Sci. Eng. A 645 (2015) 65–71.
[17] X.D. Xu, P. Liu, S. Guo, A. Hirata, T. Fujita, T.G. Nieh, C.T. Liu, M.W. Chen, Acta Mater. 84 (2015) 145–152.
[18] N.G. Jones, K.A. Christofidou, H.J. Stone, Mater. Sci. Technol. 31 (2015) 1171–1177.
[19] C. Ng, S. Guo, J. Luan, S. Shi, C.T. Liu, Intermetallics 31 (2012) 165–172.
[20] N.G. Jones, J.W. Aveson, A. Bhowmik, B.D. Conduit, H.J. Stone, Intermetallics 54 (2014) 148–153.
[21] N.G. Jones, A. Frezza, H.J. Stone, Mater. Sci. Eng. A 615 (2014) 214–221.
[22] J.W. Elmer, T.A. Palmer, E.D. Specht, Metall. Mater. Trans. A 38 (2007) 464–475.
[23] R. Magnabosco, Mater. Res. 12 (2009) 321–327.
[24] A. Oradei-Basile, J.F. Radavich, in: E.A. Loris (Ed.), Superalloys 718, 625 and Various Derviatives, 1991, pp. 325–335.
[25] R.C. Reed, M.P. Jackson, Y.S. Na, Metall. Mater. Trans. A 30 (1999) 521–533.